Supplementary Information

Literature selection, model definitions, calculation inputs and reproducibility

Bubbling Fluidized Bed Reactors for CaO-Based CO_2 Capture with Geldart Group B Particles: A Critical Review of the Coupling Between Bubble Hydrodynamics, High-Temperature Heat Transfer and Carbonation Performance

This supplement documents the targeted literature extension and calculations supporting the revised review. All new numeric results are deterministic screening calculations. No ranges are statistical confidence intervals, and no generated result is an experimental observation. Existing-source citations refer to the manuscript bibliography unless a direct source URL is supplied.

S1. Literature Scope and Evidence Provenance

The submitted manuscript reported a search through 24 August 2026. The revision added a targeted narrative web search on 27 September 2026 using exact titles, authors, application terms, publisher records and institutional copies. This was not a systematic database review: no exhaustive hit count, Scopus/Web of Science search or formal exclusion flow is claimed. Full texts were inspected when accessible; descriptions based on publisher abstracts or institutional metadata are limited accordingly.

A Direct reacting CaO/CaCO3 bubbling-fluidized-bed measurements.

B Inert or nonreacting Group-B measurements and supporting hot-limestone hydrodynamics where controlled reaction state is not established.

C Measurements in other reacting fluidized systems.

D Numerical simulation, mechanistic inference and calculations in the present review.

Table S1. Established CaL model precedents and scope of transfer to the present review.

Study	Configuration	Coupling and validation	Relevance and limits
Shimizu et al. [15]	Twin fluidized-bed process; BFB absorber	Material and heat balances with absorber kinetic/BFB sizing; tube arrangement can determine height.	Early BFB thermal–reaction design precedent; coupling itself is not new.
Hawthorne et al. [75]	CFB carbonator in a dual-bed process	Conference reactor-model precedent identified in the co-author's institutional bibliography.	Historical placement only here; original proceedings text was not inspected.
Lasheras et al. [72]	1D CFB carbonator coupled to plant simulation	K–L hydrodynamics, circulation, inventory and make-up sensitivity.	Established reactor/process coupling; not a resolved tube-bank BFB model.
Charitos et al. [17]	Two experimental CFB carbonators	Active-space-time model compared with continuously circulating facilities.	Supports inventory/reactivity coupling; does not validate the present BFB exchange closure.
Romano [16]	K–L-based CFB carbonator	Hydrodynamic description combined with sorbent kinetics and capacity.	Established coupled reactor modelling; regime-specific calibration remains necessary.
Diego et al. [73]	Interconnected CFB carbonator/calciner	Circulation and inventory model tests compatibility of capture and hydrodynamic demands.	Solids-loop feasibility is an existing design problem; not a BFB bubble closure.
Ylätalo et al. [74]	Dynamic 1D interconnected reactors	Mass, energy and conversion equations; comparison with a 30 kW facility.	Energy–hydrodynamics–reaction coupling predates this review.

Study	Configuration	Coupling and validation	Relevance and limits
Hornberger et al. [22]	200 kW pilot; BFB carbonator–CFB calciner	Reacting performance and active-space-time modelling under cement-related conditions.	Experimental architecture precedent; fitted apparent rates are not universal intrinsic constants.
Guo et al. [18]	Reactive BFB with immersed tubes; TFM	Flow, reaction and heat-transfer simulation with operating-condition sensitivity.	Explicit reactive/thermal BFB coupling exists; predicted renewal feedback requires targeted experimental testing.
Song et al. [56,57]	Confined grain-to-reactor CFD–DEM	Carbonation/heat-transfer model and vibration-induced structured bubbling simulations.	Contemporary bubble–reaction coupling; submodel comparisons do not establish unconstrained industrial-bed validation.
Present review	BFB-focused narrative synthesis	Transparent screening calculations, evidence classification and sensitivity analysis.	Organises interacting limits and validation needs; no new experimental validation or priority claim.

Generic coupled-model history is also relevant: Ding and Gidaspow [51] supplied a two-fluid granular-flow model; Theologos and Markatos [10] coupled FCC flow and heat transfer, and their subsequent work [11,12] included reaction. The fluidized-bed dryer study [52] addressed transport coupling. Tsuji et al. [53], Kaneko et al. [54], Xue and Fox [19], and Wang and Shen [55] provide discrete-particle, reacting-particle, variable-density and coarse-graining precedents. These applications establish methodology without validating CaL-specific closures.

Hawthorne et al. [75] is a bibliographically verified proceedings precedent; detailed closure claims are not inferred from metadata alone.

S2. Search Record and Source Access

The following query families were actually used in the revision. Variations with exact titles, DOI strings and publisher domains were used to verify the resulting records.

Table S2. Targeted query families used on 27 September 2026.

Topic	Queries and Terms
Historical fluidization	Theologos Markatos 1992 1993 flow heat transfer fluid catalytic cracking; reacting fluidized bed two-phase model; fluidized-bed drying; reacting DEM; variable particle density; coarse-grained CFD-DEM
CaL models	Shimizu twin fluid-bed reactor; Romano 2012 carbonator; Lasheras Ströhle Galloy Epple 2011; Charitos Hawthorne carbonator hydrodynamics; Diego Abad carbonator model; Ylätalo calcium looping
Particle properties	Tregambi solar-driven calcium looping fluidized beds thermochemical energy storage; Di Lauro fluidised bed inventory limestone density; high temperature micro fluidization of limestones
Heat transfer and exchange	Chen high-temperature fluidized bed heat transfer; Guo horizontally immersed tubes Geldart B; Molignano dense fluidized beds mass transfer; Xie bubble emulsion high temperature
Closure and equilibrium verification	Mori Wen estimation bubble diameter; Werther gas distributor hydrodynamics; Jaiswal bubble correlations; Hornberger tail-end calcium looping carbonation; Silcox flash calcination model

Primary source access is recorded below for the additions central to the revision. DOI resolution failures were not treated as proof that an article did not exist. Bibliographic verification alone was not treated as full-text verification.

S3. Provenance of Equations and Illustrations

Table S3. Classification of relations and contributions.

Item	Provenance	Interpretation
Equilibrium and Wen–Yu relations	Established literature relations	Specified units and validity ranges retained
Darton, Mori–Wen, Werther and K–L exchange	Established empirical/model closures	Transferred to hot CaL only as sensitivity assumptions
Four-constraint representation	Review synthesis of established limits	Not a new conservation law or universal predictive equation
Constant-envelope trajectory	Stoichiometric calculation under stated geometry	Conceptual property scenario; not a measured trajectory
Common initial bubble size	Explicit comparison normalization	Virtual origins changed to compare growth from 2 cm
Coupled crossover model	New illustrative phenomenological calculation	One gas route and uniform temperature; no full two-phase validation
Tube-bank layout and stage resets	Illustrative engineering scenarios	No experimentally demonstrated bubble cap or optimal stage depth
Dimensionless diagnostics	Established time-scale concepts and defined ratios	Dimensions stated; not new validated similarity laws

S4. Thermodynamic and Molar-Flow Calculations

For CO_2 removal only, inert molar flow is conserved. Capture is $E = (F_{CO_2,in} - F_{CO_2,out})/F_{CO_2,in}$, giving $y_{out} = y_{in}(1 - E)/(1 - y_{in} E)$. Substituting $y_{eq} = p_{eq}/P$ yields the exact contraction-corrected equilibrium bound below. The bound is clipped to zero when $y_{eq} \geq y_{in}$ and to the physical interval 0–1.

$$y_{out} = \frac{y_{in}(1-E)}{1-y_{in}E}, E_{eq} = \max\left[0, \frac{y_{in}-y_{eq}}{y_{in}(1-y_{eq})}\right]$$

$$p_{eq}/\text{atm} = 4.137 \times 10^7 \exp(-20474/T)$$

$$p_{eq}/\text{bar} = 4.0009 \times 10^7 \exp\left(\frac{-169500}{RT}\right)$$

The first expression is attributed to Silcox et al. [21]. The second is the FactPS-derived fit reported in Hornberger et al. [22], equation 4, over 500–1000 °C. R = 8.314462618 J mol^{-1} K^{-1}; T is in kelvin. Calculations use P = 101325 Pa, with 1 bar = 100000 Pa. Their separation is a comparison between published representations, not a calibrated thermodynamic uncertainty bound. No new FactPS database run was performed.

Files: table1_equilibrium.csv and figure2_thermodynamics.csv. The plotted 500–800 °C range stays inside the stated independent-fit temperature range. No direct-air-capture extrapolation below that range is presented.

S5. Particle-Property Construction and Propagation

For one mole of retained Ca, use M_{CaO} = 0.056077 kg mol^{-1}, M_{CO_2} = 0.0440095 kg mol^{-1}, $V_{CaO} = 16.9 \times 10^{-6}$ m^3 mol^{-1} and $V_{CaCO_3} = 36.9 \times 10^{-6}$ m^3 mol^{-1}. The reference particle is initially nonporous pure calcite with d_0 = 300 μm. At conversion X and diameter multiplier α, its envelope volume is $V_{CaCO_3}\,\alpha^3$.

$\rho_{env} = (M_{CaO} + X\,M_{CO_2})/(V_{CaCO_3}\,\alpha^3)$; $d_p = d_0\alpha$; $\varepsilon_p = 1 - [(1 - X)V_{CaO} + XV_CaCO_3]/(V_{CaCO_3}\,\alpha^3)$. The baseline uses $\alpha = 1$. The chosen $\alpha = 0.9$ and 1.1 cases are mass-conserving diameter sensitivities. Negative porosity is excluded. Fragmentation and selective fines removal are not represented by these same-mass diameter changes.

Wen–Yu is implemented as $Ar = d_p^3\rho g(\rho_{env} - \rho g)g/\mu^2$, $Re_mf = [33.7^2 + 0.0408Ar]^{1/2} - 33.7$, and $U_mf = Re_mf\,\mu/(\rho g\,d_p)$. At 650 °C, $\mu = 3.8 \times 10^{-5}$ Pa s and $\rho g = 0.38$ kg m^{-3} are assumed air-like properties. Propagation uses Darton growth with $U_0 = 0.5$ m s^{-1} and $A_0 = 10^{-4}$ m^2; K_{be} is shown at $z = 0.5$ m and exchange is integrated over $H = 1$ m.

Table S4. Calculated property propagation at the fixed-envelope baseline.

X	ρ_{env} (kg m^{-3})	U_mf (m s^{-1})	d_b at 0.5 m (m)	K_{be} (s^{-1})	Integrated E_b (%)
0.00	1520	0.02135	0.1556	0.638	66.3
0.10	1639	0.02302	0.1554	0.645	66.7
0.20	1758	0.02470	0.1552	0.652	67.2
0.50	2116	0.02972	0.1545	0.671	68.4

Experimental comparison is qualitative and observable-specific. Tregambi et al. [38] measured hot U_mf after reaction steps; Di Lauro et al. [39] measured size distributions, porosimetry and poured bulk density. Poured bulk density includes interparticle packing and cannot validate the particle-envelope density used in drag without a separate voidage measurement. A joint particle size–conversion–cycle distribution is needed where a representative particle is inadequate.

S6. Bubble Growth and Exchange Calculations

Common inputs are T = 650 °C, P = 1 atm, $U_mf = 0.0225$ m s^{-1}, $D_{CO_2} = 1.2 \times 10^{-4}$ m^2 s^{-1}, $\varepsilon_mf = 0.50$ and column diameter $D_c = 1$ m. The primary correlation comparison uses $U_0 = 0.25$ m s^{-1}. The $U_0 = 0.5$ m s^{-1} Werther comparison is marked as velocity extrapolation. All correlations require additional validation for hot reacting CaL.

Darton is $d_b = 0.54(U_0 - U_mf)\text{^}0.4(z + 4\sqrt{A_0})\text{^}0.8/g\text{^}0.2$ in SI units, with native $A_0 = 10^{-4}$ m^2 per orifice. Mori–Wen is $d_b = d_{bm} - (d_{bm} - d_{b0})\exp(-0.3z/D_c)$. Its native empirical coefficients are $d_{bm} = 0.652[A(U_0 - U_mf)]\text{^}0.4$ and $d_{b0} = 0.00376(U_0 - U_mf)^2$, using centimetres, square centimetres and centimetres per second before conversion to SI. The latter initial-size formula represents a porous distributor.

The Group B Werther form is $d_b[cm] = 0.853[1 + 0.272(U_0 - U_mf)[cm\ s^{-1}]]\text{^}(1/3)[1 + 0.0684z[cm]]\text{^}1.21$. The formula and unit conventions were cross-checked in the primary comparative study of Jaiswal et al. [43]. The original Werther record was verified bibliographically, not inspected as an original full text. The selected 0.25 m s^{-1} comparison lies within the commonly cited 5–30 cm s^{-1} excess-velocity range, but this does not validate its temperature or reacting application.

Figure 4 uses a common initial $d_{b0} = 0.02$ m. Write Darton as $C(z + z_0)\text{^}0.8$ and choose $z_0 = (0.02/C)\text{^}1.25$. Write Werther as $C(1 + 6.84z)\text{^}1.21$ in SI and choose virtual $z_v = [(0.02/C)\text{^}(1/1.21) - 1]/6.84$, evaluating at $z + z_v$. Mori–Wen uses imposed $d_{b0} = 0.02$ m directly. This is an explicitly normalized growth comparison; it changes the native distributor condition. Both native and normalized results are supplied.

Rise velocity is $u_b = U_0 - U_mf + 0.711\sqrt{(g d_b)}$. Exchange uses $K_{bc} = 4.5U_mf/d_b + 5.85D\text{^}0.5g\text{^}0.25/d_b\text{^}1.25$, $K_{ce} = 6.77(\varepsilon_mf\,D\,u_b/d_b^3)\text{^}0.5$ and $K_{be} = (1/K_{bc} + 1/K_{ce})^{-1}$. Both K coefficients have units s^{-1}. N_x is the integral of local K_{be}/u_b over z. Applying the outlet diameter over the entire bed is a different and generally more pessimistic approximation.

$$E_b = 1 - \exp(-N_x), N_x = \int_0^H \frac{K_{be}(z)}{u_b(z)}\,dz$$

$$E_{h,0} = \frac{U_{mf}}{U_0} + \left(1 - \frac{U_{mf}}{U_0}\right) E_b$$

K_{be} multipliers 0.5, 1 and 2 and u_b multipliers 0.85, 1 and 1.15 define selected sensitivity scenarios. K_{ce} is recalculated using the varied velocity. They are not probability distributions. In the common-initial comparison, the baseline integrated bubble-route depletions at H = 1 m are 83.0%, 81.5% and 89.9% for Darton, Mori–Wen and Werther.

Table S5. Common-initial-diameter comparison at H = 1 m.

Closure	U_0 (m s^{-1})	Top d_b (cm)	Integrated E_b (%)	Validity note
Darton	0.25	19.8	83.0	Hot reacting use unvalidated
Darton	0.5	26.3	66.0	Hot reacting use unvalidated
Mori–Wen	0.25	22.8	81.5	Hot reacting use unvalidated
Mori–Wen	0.5	30.2	65.2	Hot reacting use unvalidated
Werther	0.25	20.4	89.9	Hot reacting use unvalidated
Werther	0.5	24.7	79.5	Velocity extrapolation

The bubble-size-distribution example uses two diameters $\bar{d}(1 - w)$ and $\bar{d}(1 + w)$, with equal gas-flux weights, w = 0, 0.3 or 0.5. Overall bubble escape is $\Sigma w_i \exp(-N_{x,i})$, not exp evaluated at a number-mean diameter. Files provide the selected distributions and results. No measured bubble distribution or chord-to-volume conversion is inferred.

S7. Staging and Idealized Internals

For the gas-route staging screen, $Y = F_{CO_2}/F_{inert}$, $y = Y/(1 + Y)$, and inert molar flux I is conserved. The equation is $dY/dz = -(K_{be}/u_b)(1 + Y)(y - y_{eq})$, limited to positive driving force, with $U = I(1 + Y)RT/P$. At each axial step the code updates U, bubble growth and exchange. Stable exponential stepping uses $Y_eq = y_{eq}/(1 - y_{eq})$.

Inputs are 650 °C, 1 atm, inlet U_0 = 0.5 m s^{-1}, y_{in} = 0.15 and Darton $A_0 = 10^{-4}$ m^2. Four equal stages reset the growth coordinate at each distributor; interstage composition and contracted gas flow are passed to the next stage. Internal scenarios impose $d_b = \min(d_{Darton}, d_{cap})$, with d_{cap} = 5 or 10 cm. These caps are not derived from the specified tube bank.

Table S6. Staging screen at a common total depth of 1 m.

Configuration	Capture (%)	Outlet CO_2 (vol %)	Outlet U (m s^{-1})
one bed	64.6	5.89	0.452
four stages	91.3	1.51	0.432
one bed db cap 5cm	90.5	1.65	0.432
one bed db cap 10cm	74.0	4.38	0.444

The comparison assumes fast uptake, adequate local active sorbent and sufficient heat removal. It omits separate emulsion flow, finite kinetics, solids backmixing, distributor pressure losses and interstage solids allocation.

Equal total bed height therefore does not establish equal practical inventory or pumping duty. A multistage design requires a specified return arrangement and stagewise solids conversion balances before these optimistic results can be tested.

S8. Supply and Reduced Coupled Crossover Model

The supply screen is $E_{supply} = \min[1, (F_R/F_{CO_2,in})\Delta X_{max}]$. Ca/C = 4–10 and ΔX = 0.10–0.15 cover 40–100% supply limits. A 90% target requires Ca/C ≥ 9 at ΔX = 0.10 or ≥ 6 at ΔX = 0.15. Figure 6a,b takes the minimum of supply, equilibrium and ideal zero-equilibrium transport screens. It is a classification map, not a solved reactor prediction.

The crossover example is a phenomenological one-gas-route model with a well-mixed bed temperature. k_r has units s^{-1} and is defined per total bed volume: $r = k_r(C_r - C_{eq})$, with activity and phase hold-up absorbed. It is not an intrinsic surface kinetic coefficient or the sorbent-normalized $k_{s\varphi}$ fitted in a different reactor model. A local quasi-steady resistance closure imposes $k_m(C_{bulk} - C_r) = k_r(C_r - C_{eq})$, where $k_m = U K_{be}/u_b$. Eliminating C_r gives $a_{eff} = [(K_{be}/u_b)^{-1} + (k_r/U)^{-1}]^{-1}$ in m^{-1}.

With F and I denoting CO_2 and inert fluxes, $dF/dz = -a_{eff}[F(1 - y_{eq}) - I\, y_{eq}]$, $U = (F + I)RT/P$. Uptake per plan area is nonnegative and cannot exceed $J_{R\Delta X}$_max, where $J_R = F_R/A$. Temperature simultaneously satisfies $J_{CO_2,in} E|\Delta H| = [haH + J_{g,in}\, C_{p,g} + G_{s,in}\, C_{p,s}](T - T_{ref})$. Here all J quantities are molar fluxes (mol m^{-2} s^{-1}), $G_{s,in}$ is the solids mass flux (kg m^{-2} s^{-1}), and A is the reactor plan area. All inlet streams and the mean wall temperature equal T_{ref} in this particular example. Reaction enthalpy is held at 178 kJ mol^{-1} as an approximation at the bed temperature, so sensible heats are consistently evaluated for the incoming streams.

Inputs: y_{in} = 0.01, P = 101325 Pa, H = 0.5 m, U_{in} = 0.25 m s^{-1} at T_{ref}, column diameter 1 m, $A_o = 10^{-4}$ m^2, Ca/C = 7.5, ΔX_{max} = 0.12, h = 300 W m^{-2} K^{-1} and a = 5 m^2 m^{-3}. $C_{p,g}$ = 33.4 J mol^{-1} K^{-1} and $C_{p,s}$ = 1000 J kg^{-1} K^{-1}. ρ_{env} is fixed at 1520 kg m^{-3}. Gas-property assumptions are $\rho g = 0.38(923.15/T)$, $\mu = 3.8 \times 10^{-5}(T/923.15)^{0.7}$ and $D = 1.2 \times 10^{-4}(T/923.15)^{1.75}$ in SI units.

At 575 °C, $k_{r,ref}$ = 0.1, 0.5 or 2 s^{-1}. The selected activation energy is 30 kJ mol^{-1}, giving $k_r(T) = k_{r,ref} \exp[-30000/R(1/T - 1/848.15)]$. This is a chosen sensitivity family, not fitted kinetics. The separate transfer screen removes finite reaction and equilibrium; the separate kinetic screen removes finite transfer and equilibrium; the supply and exact equilibrium limits are imposed separately. A conditional thermal screen permits a 20 K rise. The minimum is then compared with the simultaneously solved mass/energy result.

Table S7. Coupled-model comparison for the selected effective-rate scenarios.

T_{ref} (°C)	$k_{r,ref}$ (s^{-1})	Minimum (%)	Isothermal coupled (%)	Thermal coupled (%)	T_{bed} (°C)
550	0.1	16.1	12.9	12.9	551.0
550	0.5	58.6	35.9	35.8	552.7
550	2	82.3	57.4	57.1	554.2
575	0.1	18.1	13.2	13.2	576.0
575	0.5	63.3	35.4	35.1	577.5
575	2	82.9	55.0	54.1	578.9
600	0.1	20.2	12.2	12.2	600.9
600	0.5	67.8	31.7	31.1	602.2
600	2	73.1	47.9	46.3	603.3

The gap demonstrates how simultaneous finite resistances differ from a minimum of isolated optimistic bounds. Its magnitude is specific to this closure and the selected inputs. A fully resolved two-phase reactor calculation and an evolving solids population were not performed. Calibration against an actual bed is required before using these results for design.

S9. Tube Geometry and Solids Circulation

The selected square stage has a 1 × 1 m plan and 0.4 m expanded depth. Twenty 1 m immersed tubes of 25 mm outside diameter form two aligned rows at 0.10 and 0.26 m elevation. Horizontal and vertical pitches are 95 and 160 mm. Tube area is 1.571 m², area density 3.927 m² m⁻³ and occupied volume 0.00982 m³ (2.45%). Tube centres and side clearances fit the assumed stage; headers, supports and differential expansion remain to be designed.

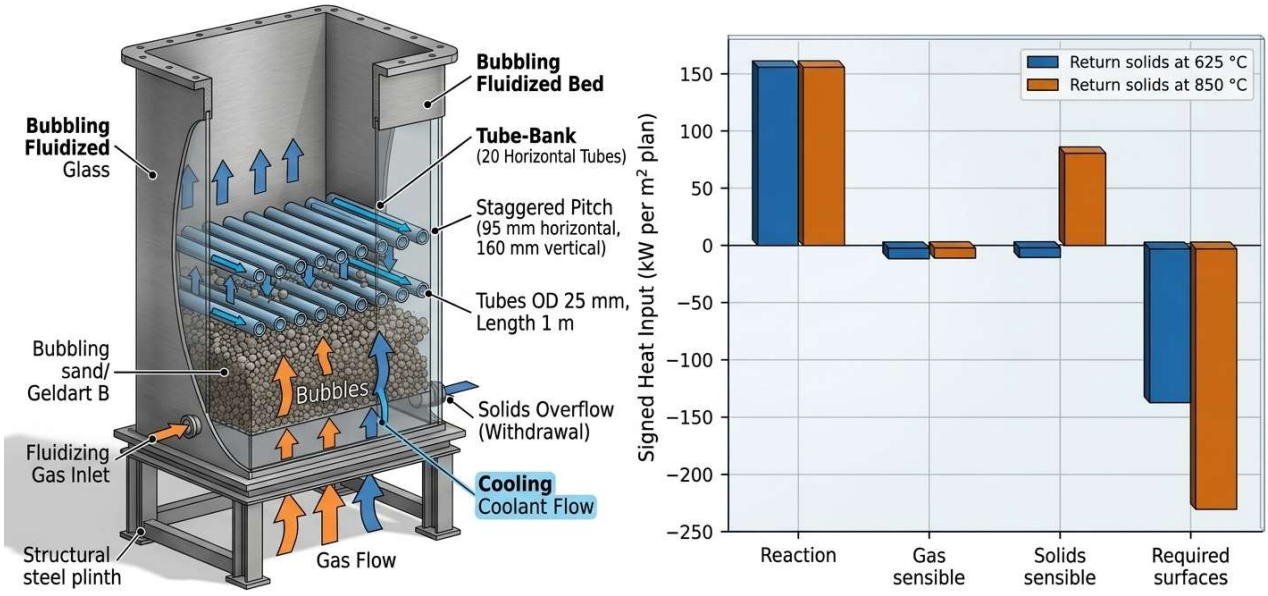


Figure S1. Illustrative tube-bank geometry and signed heat-balance scenarios. The arrangement is a feasibility example, not an as-built design or a validated bubble-breakup closure.

At 650 °C, 1 atm, inlet U_0 = 0.5 m s⁻¹ and 15% CO_2, inlet CO_2 is 0.9901 mol s⁻¹. Ca/C = 7.5 gives 7.426 mol Ca s⁻¹. A 90% target needs ΔX = 0.12, corresponding to 0.416 kg s⁻¹ incoming CaO and 0.456 kg s⁻¹ outgoing partially carbonated solids. For a well-mixed X = 0.12 bed, assumed bubble hold-up 0.35 and emulsion voidage 0.50, $M_s = (V - V_{tube})(1 - \delta_b)(1 - \varepsilon_e)\rho_{env}$ = 210.9 kg. n_{Ca}/F_R = 463 s, or 7.7 min.

An external dense-phase withdrawal and regenerated-solids return must provide this flow. Hornberger et al. [22] offer a BFB-carbonator/CFB-calciner experimental precedent, but the present stage is not a reproduction of that pilot. With make-up $F_0/F_{CO_2,in}$ = 0.05 and equal-probability purge, F_0/F_R = 0.00667 and mean passes before purge are 150. A real age/size/attrition distribution must support the assumed ΔX; the make-up ratio alone does not establish it.

The heat balance uses a constant reaction enthalpy approximated at bed temperature and incoming-stream sensible enthalpies: $Q_{rxn} = Q_{surface} + F_{g,in}\, C_{p,g}(T_b - T_{g,in}) + \dot{m}_{s,in}\, C_{p,s}(T_b - T_{s,in})$, neglecting losses. At $T_{g,in}$ = 600 °C the gas sink is 11.0 kW. Return solids at 625 °C remove 10.4 kW, whereas return at 850 °C supplies 83.3 kW. Required surface duties are therefore 137.2 and 230.9 kW, respectively.

With h = 500 W m⁻² K⁻¹ and wall temperature 350 °C, surface capacity is 235.6 kW. The hot-return case has little margin and fails if h falls to 300 W m⁻² K⁻¹. A detailed design must use temperature-dependent enthalpies,

actual steam-side conditions, heat losses, return-cooler duty, erosion constraints and coupled tube-bank hydrodynamics.

Figure 7 deliberately tests h = 500(U₀/0.5)^s with s = −0.5, 0 and +0.5. These are assumed negative, flat and positive slopes, not fitted correlations. The surface-only reaction-duty ratio is q‴/(haΔT), equivalently Q_{rxn}/(hA_htΔT). For an actual balance, use $Q_{surface,required}$ in the numerator after sensible heat contributions. Multiplying the volumetric expression by H would incorrectly give dimensions of length.

S10. Reproduction and Numerical Verification

Run calculations.py with Python 3 to regenerate the table and figure CSVs and results.json. The calculation script uses the Python standard library only. Run plot_figures.py with NumPy and Matplotlib to regenerate the PNG, SVG and PDF figures. SVG text remains editable. The figure script reads the accompanying CSV data; its output is not an AI-generated raster illustration.

Table S8. Figure data map.

Figure	Data file	Definition
2	figure2_thermodynamics.csv	Published equilibrium representations and corrected capture
3	figure3_density_sensitivity.csv	Linked diameter/density scenarios and propagated transport
4	figure4_matched_correlation_sensitivity.csv	Shared 2 cm initial bubble size; scenario envelopes
5	figure5_staging_internals.csv	Composition and flow updated between axial steps/stages
6a,b	figure6a_supply_map.csv	Conditional supply and transport classification
6c	figure6b_coupled_crossover.csv	Selected k_r = 0.5 s^{-1} panel from all supplied scenarios
7	figure7_velocity_thermal_scenarios.csv	Assumed h slopes and reaction-duty ratio
S1	results.json / tube_bank	Geometry and signed sensible-heat contributions

The numerical checks verify capture fractions in 0–1, equilibrium inert-flow conservation, containment of baseline values within the selected exchange scenarios, matching 2 cm initial bubble sizes, tube clearances and energy-balance residuals. Step refinement is recorded in verification.json. These checks establish numerical consistency of the defined model, not physical validation. The complete calculation and figure sources accompany this supplement.